JOURNAL OF AIRCRAFT
Vol. 29, No. 5, Sept.–Oct. 1992

Flutter and Stall Response of a Helicopter Blade with Structural Nonlinearity

D. M. Tang* and E. H. Dowell†
Duke University, Durham, North Carolina 27706

The purpose of the present paper is to study the flutter instability and forced response of a nonrotating helicopter blade model with a NACA-0012 airfoil and a pitch freeplay structural nonlinearity. In this paper, three typical combinations of linear and nonlinear structure with a linear and nonlinear (ONERA) aerodynamic model are considered. Characteristic results are used to display the limit cycle oscillation and chaotic behavior of both the flutter instability and forced response for all three cases. The effects of various initial disturbance amplitudes on the forced response behavior are discussed. Comparisons of the results for the three cases are helpful in understanding physically the nonlinear aeroelasticity phenomena and chaotic oscillations.

Nomenclature

a_{0l} = blade section linear lift curve slope
$b, \bar{b}$ = blade semi-chord, b/R
C_l, C_m = section lift, pitch moment coefficient
$c, \bar{c}$ = blade chord, c/R
I_β = blade rotational inertia
$I_f, \bar{I}_f$ = blade pitch inertia, I_f/I_β
$I_y, \bar{I}_y$ = inertial flap-pitch coupling, I_y/I_β
$K_\beta, K_{\phi s}$ = flap hinge spring, pitch spring constant
K_ϕ = $\omega_\phi^2 \bar{I}_f$
L = section aerodynamic lift force
M_0 = section aerodynamic pitch moment about $\frac{1}{4}$ chord
m = blade mass per unit length
N = number of aerodynamic elements
R = rotor radius
$r, \bar{r}$ = radial location on the blade measured from the center of rotation, r/R
$r_i, \bar{r}_i$ = distance from rotor center to center of ith aerodynamic section, r_i/R
t, t_r = time, b/U
U = freestream velocity
$y_{ac}, \bar{y}_{ac}$ = aerodynamic center of blade section from the pitch axis, y_{ac}/c
$y_{am}, \bar{y}_{am}$ = center of gravity of blade section from the pitch axis, y_{am}/c
α = blade section angle of attack
β = the degree of freedom for the flap motion
Δ_i = dimensionless width of ith aerodynamic section
γ = blade Lock number, $ac\rho R^4/I_\beta$
θ_{con} = pitch control input, $\theta_0 + \theta_s \sin \Omega t$
θ_s = excitation amplitude in pitch angle
θ_0 = initial pitch angle
μ = amplitude ratio of ϕ_L to ϕ_a
ρ = air density
τ = reduced time, tU/b
ϕ = the degree of freedom for the pitch motion
ϕ_a = the magnitude of deadspace in pitch
ϕ_L = the limit cycle amplitude in pitch
ϕ_p = the static deviation pitch angle
Ω = excitation frequency
$\omega_\beta, \omega_\phi$ = flap, pitch natural frequency, $\sqrt{K_\beta/I_\beta}$, $\sqrt{K_{\phi s}/I_f}$
$( )'$ = d( )/dt

Received Oct. 31, 1990; revision received Sept. 16, 1991; accepted for publication Sept. 23, 1991.

*Research Associate, Department of Mechanical Engineering and Materials Science.
†Dean, School of Engineering. Fellow AIAA.

I. Introduction

RECENTLY nonlinear aeroelastic problems have attracted many investigators' attention. References 1–3 used a nonlinear aerodynamic stall model to investigate both stability and stall response of a helicopter blade and cantilevered Graphite/Epoxy wings; but the blade and wing structural configurations were assumed to be linear. References 4 and 5 conducted analytical and experimental aeroelastic investigations of airfoil surfaces with structural nonlinearities, but the aerodynamic model was assumed to be linear. References 2 and 6 presented interesting experimental results which demonstrated chaotic motion behavior for a nonlinear aeroelastic system. These studies have shown that nonlinearities influence not only the flutter speed, but also the characteristics of the flutter motion.

The purpose of the present article is to study flutter instability and forced response of a nonrotating helicopter blade with structural nonlinearity and the nonlinear ONERA stall aerodynamic model. In order to compare the results obtained from the present analytical prediction with those obtained from the companion experiment,[2] the analytical model and parameters are taken to be similar to those of the experimental model. The external excitation is similar to the blade cyclic pitch control input from a swashplate of the helicopter.

In this article, three cases are considered: case A, a nonlinear blade structure with a linear aerodynamic model; case B, a linear blade structure with an ONERA nonlinear aerodynamic model; and case C, a nonlinear blade structure with the ONERA model. Characteristic results obtained from theory are used to display the limit cycle oscillation and chaotic behavior of both the flutter instability and forced response for all three cases. The effects of various initial disturbance amplitudes on the forced response behavior are also discussed. Comparisons of the results for the three cases are helpful in understanding physically the nonlinear aeroelasticity phenomena and chaotic oscillations.

II. Equations of Motion

The present study is based upon a consistently derived system of equations of motion for the coupled flap-pitch motion of an experimental wind-tunnel model rotor blade section without rotation as shown in Fig. 1. The nonlinear effects are incorporated in the aerodynamic stall model and nonlinear pitching stiffness of the blade configuration. The blade airfoil

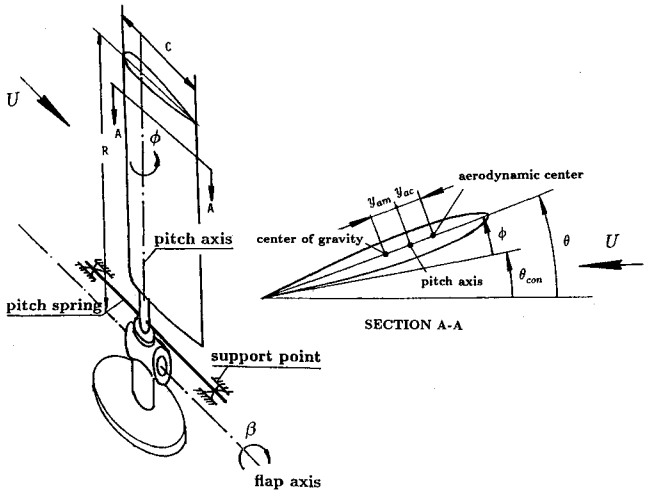

Fig. 1 Experimental model.

section aerodynamic lift force and pitch moment about ¼ chord per unit span length are given by simple expressions based on two-dimensional airfoil coefficients:

$$L = \tfrac{1}{2}\rho c C_z U^2 \tag{1}$$

$$M_0 = \tfrac{1}{2}\rho c^2 C_m U^2 \tag{2}$$

A semiempirical theoretical aerodynamic model, the ONERA model, is used in the present paper. This model describes dynamic stall in terms of differential equations. The ONERA aerodynamic model yields both the lift and moment coefficients of each blade section and is described in terms of a reduced time (d/dτ, $\tau = Ut/b$). These are not convenient for the dynamic analysis of the blade; however, a more conventional differential operator relative to the real time, d/dt, is used in this article for comparison with the experimental data. This is given by

$$\mathrm{d}/\mathrm{d}\tau = b/U\ \mathrm{d}(\ )/\mathrm{d}t = t_\tau(\ )' \tag{3}$$

By considering the effects of pitch rate and plunge on unsteady airfoil behavior, the modified form of the ONERA model used for this study is represented by

$$C_z = C_{za} + C_{zb} \tag{4}$$

$$C_{za} = t_\tau s_z \alpha' + t_\tau^2 k_{vz}\theta'' + C_{z\gamma} \tag{5}$$

$$t_\tau C'_{z\gamma} + \lambda_z C_{z\gamma} = \lambda_z(a_{0z}\alpha + t_\tau \sigma_z \theta') + \alpha_z(t_\tau a_{0z}\alpha' + t_\tau^2 \sigma_z \theta'') \tag{6}$$

$$t_\tau^2 C''_{zb} + 2t_\tau\, \mathrm{d}\omega C'_{zb} + w^2(1 + \mathrm{d}^2)C_{zb} = -w^2(1 + \mathrm{d}^2)\left(\Delta C_z + t_\tau e \frac{\partial \Delta C_z}{\partial \alpha}\alpha'\right) \tag{7}$$

C_z represents either the relevant nondimensional lift force coefficient C_l or the pitch moment coefficient C_m. The coefficients, λ_z, σ_z, d, w, and so forth, of these equations were determined by parameter identification using the wind-tunnel test data, see Petot and Dat.[7] References 3 and 7 contain an in-depth discussion of the basis for the ONERA model.

The ONERA dynamic stall model is based on a blade airfoil element. Here, it is applied to a single blade flap-pitch motion problem. A simple assumption is that the blade is divided into N aerodynamic sections, and the ONERA model is applied to each section. The equations of motion for a rigid, articulated blade are given by

Table 1

Parameter	Numerical value
R	0.5 m
c	0.1 m
b	0.05 m
ω_β	15 Hz
ω_ϕ	30 Hz
γ	1.588
y_{am}	0.005 m
y_{ac}	−0.005 m
I_β	3.757×10^{-3} kgms^2
I_y	5.6355×10^{-5} kgms^2
I_f	0.939×10^{-5} kgms^2

$$\beta'' + \omega_\beta^2\beta - \bar{I}_y\phi'' = \frac{\gamma}{2a_{0l}R^2}\sum_i^N \Delta_i \bar{r}_i C_{li} U_i^2 \tag{8}$$

$$\bar{I}_f\phi'' + K_\phi\phi - \bar{I}_y\beta'' = \frac{\gamma\bar{c}}{2a_{0l}R^2}\sum_i^N \Delta_i U_i^2[C_{mi} - \bar{y}_{ac}C_{li}] + K_\phi\theta_{\mathrm{con}} \tag{9}$$

For the ith blade section, the variable C_{la}, C_{lb}, C_{ma}, and C_{mb} should have a subscript i in Eqs. (4)–(7).

From kinematics, it can be determined that (see Fig. 1)

$$\theta = \theta_{\mathrm{con}} + \phi = \theta_0 + \theta_s \sin \Omega t + \phi \tag{10}$$

$$U_{Pi} = \theta U - r_i\beta' \tag{11}$$

$$U_{Ti} = U + r_i\theta\beta' \tag{12}$$

$$\alpha_i = \tan^{-1}(U_{Pi}/U_{Ti}) \tag{13}$$

$$\alpha'_i = [(U'_{Pi}U_{Ti} - U'_{Ti}U_{Pi})/U_i^2] \tag{14}$$

The baseline parameters are summarized in Table 1.

III. Numerical Investigation

A. Case A (Nonlinear Blade Structure with Linear Aerodynamics)

1. Stability Boundary ($\theta_s = 0$)

The structural nonlinearity of the blade is in the support stiffness such as that due to a loose hinge, or linkage of a control system, or possible joint slippage in the helicopter control system. All of these can be modeled as freeplay structural nonlinearity. The stiffness of a freeplay nonlinearity can be expressed as

$$K_\phi = \begin{cases} 0 & -\phi_a < \phi < \phi_a \\ K_{\phi s}/I_\beta & \text{otherwise} \end{cases} \tag{15}$$

Because there is an initial pitch angle θ_0, in general, the NACA 0012 airfoil section is subjected to a preload moment due to the free stream velocity field. Hence a static deviation angle ϕ_p exists and the pitching stiffness curve is not symmetric with respect to the blade angle relative to the free stream velocity. The deviation angle is dependent upon U and θ_0. The expression for the deviation angle can be obtained from Eq. (9), and is given by (note there are two possible values of ϕ_p)

$$\phi_{p+,-} = (\theta_0 \pm \phi_a)Q/(K_\phi - Q) \pm \phi_a \tag{16}$$

in which

$$Q = -\bar{y}_{ac}\gamma\bar{c}U^2/2R^2 \tag{17}$$

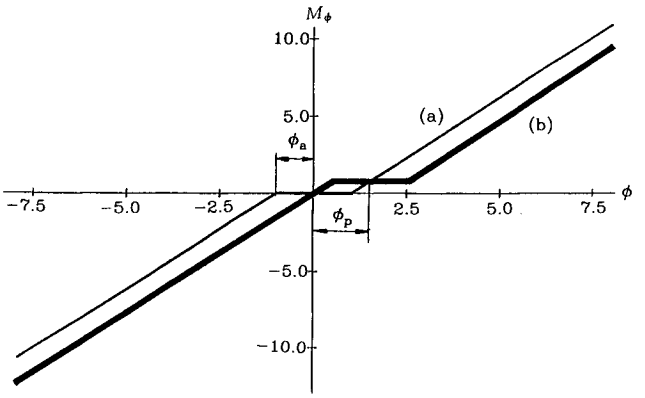

Fig. 2 Freeplay stiffness curves for ϕ_a = 1 deg: a) for θ_0 = 0 deg; b) for θ_0 = 3 deg, and U = 15 m/s.

The freeplay stiffness curve with a preload nonlinearity is shown in Fig. 2 for θ_0 = 3 deg and U = 15 (m/s).

Substituting Eq. (15) [or (16)] into Eqs. (8) and (9), a set of nonlinear equations of motion is obtained. The pitching stiffness characteristics change with the motion due to the freeplay nonlinearity. Therefore, the flutter speed (speed for neutral stability) is a function of the amplitude of oscillation. A flutter problem with structural nonlinearities is often analyzed with a linearization technique—the harmonic balance method or so called "describing function" approach. For a nonlinear pitching stiffness with freeplay characteristics, the describing function is dependent upon the magnitude of the freeplay and the amplitude of the displacement. An equivalent stiffness $K_{\phi eq}$ and an effective pitching natural frequency are defined as

$$K_{\phi eq} = \delta K_{\phi s} \tag{18}$$

$$\omega_{\phi eq} = \sqrt{\delta \omega_\phi} \tag{19}$$

The describing function δ is derived and given in Refs. 5 and 8. The linearization approach for the nonlinear flutter equations is discussed next.

a. For θ_0 = 0. A linear aerodynamic theory and the equivalent stiffness $K_{\phi eq}$ is used in Eqs. (5), (8), and (9). Thus a relationship between $K_{\phi eq}$ and U is obtained:

$$f_1 U^4 + (f_2 K_{\phi eq} + f_3) U^2 + f_4 K_{\phi eq}^2 + f_5 K_{\phi eq} + f_6 = 0 \tag{20}$$

The coefficients f_1, f_2, . . . of Eq. (20) are given in the Appendix.

A limit cycle amplitude of pitch motion, ϕ_L is first selected. The describing function δ can then be determined following Refs. 5 and 8. The corresponding equivalent pitching stiffness and the flutter critical speed are then obtained from Eqs. (18) and (20), respectively. This procedure is then repeated for other values of ϕ_L. Finally, a curve of the flutter critical speed vs the ratio of limit cycle flutter amplitude, μ, is drawn for a given linear pitching stiffness or pitching natural frequency as shown in Fig. 3 for ϕ_a = 1 deg and θ_0 = 0 deg. Note that the *ao* section of the solid line is the unstable limit cycle region. The bifurcation point *o* depends on the parameters of the system. In addition to the flutter and divergent instability boundaries for the system with a structural nonlinearity, the instability boundaries of the linear system are also drawn in this figure for a comparison. The latter are shown as asymptotes when the ratio μ approaches infinity. From Fig. 3, it is found that the flutter critical speed for a system containing a structural nonlinearity with freeplay pitching stiffness and θ_0 = 0 deg is lower than that of the linear system, in general. This is because increasing the limit cycle amplitude results in an increase of the equivalent stiffness and the flutter critical

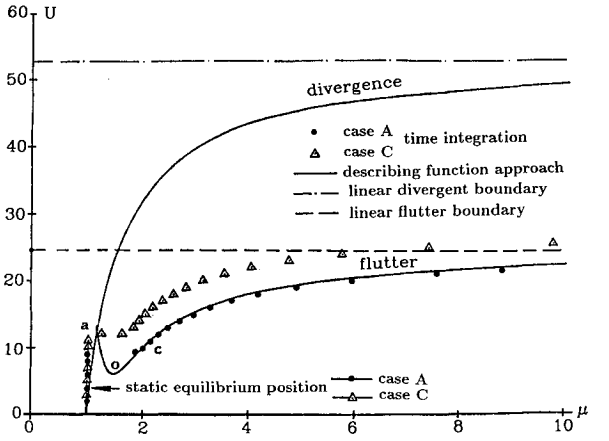

Fig. 3 Instability boundary for case A and θ_0 = 0.

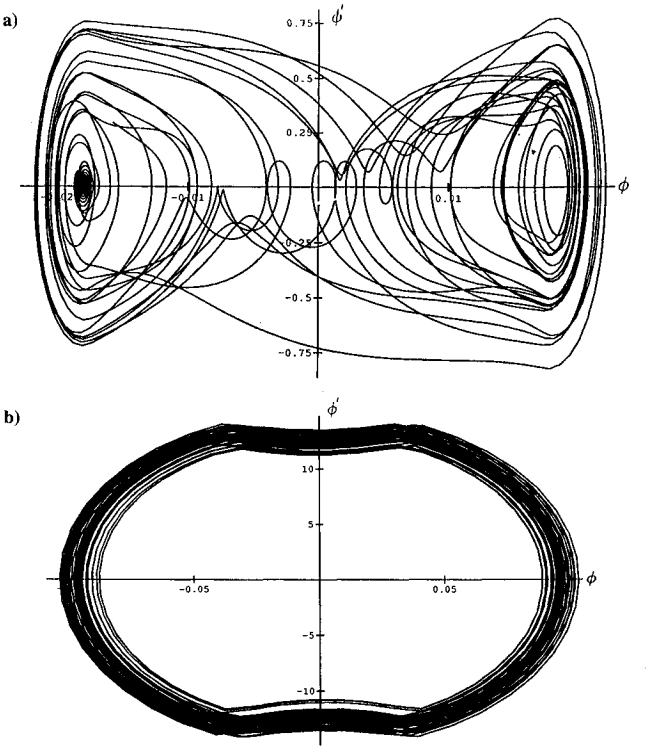

Fig. 4 Phase plane plot of pitch motion in case A: a) for U = 9.5 m/s, and $\phi(0)$ = 0.1; b) for U = 20 m/s, and $\phi(0)$ = 0.1.

speed; however, the stable limit cycle response no longer holds as the velocity for divergent oscillations is reached.

A numerical integration of the nonlinear flutter Eqs. (8) and (9) may be used to yield time history information to compare with results from the linearization approach deduced by the describing function technique. Typical results are shown in Fig. 3 for case A and case C (to be discussed later). It is shown in Fig. 3 that an amplitude-sensitive region exists (*aoc* section) for limit cycle flutter due to an initial disturbance. For case A and U = 10 m/s, when $\phi(0) \leq 0.045$ rad, the motion is convergent to unity without oscillation (i.e., $\phi \rightarrow \phi_a$), and when $\phi(0) > 0.045$ rad, the motion tends to a stable limit cycle oscillation with μ = 1.979. For case C and U = 12 m/s, when the initial value $\phi(0) \leq 0.035$ rad, the limit cycle flutter amplitude ratio μ is 1.231. However, when $\phi(0)$ = 0.05 rad, μ is equal to 1.596. When the freestream velocity U exceeds 13 m/s (beyond the sensitive region), limit cycle flutter will occur regardless of the magnitude of the initial disturbance for both cases.

Figs. 4a and 4b show the phase plane plots from the time integration results for case A, and an initial value, $\phi(0)$ =

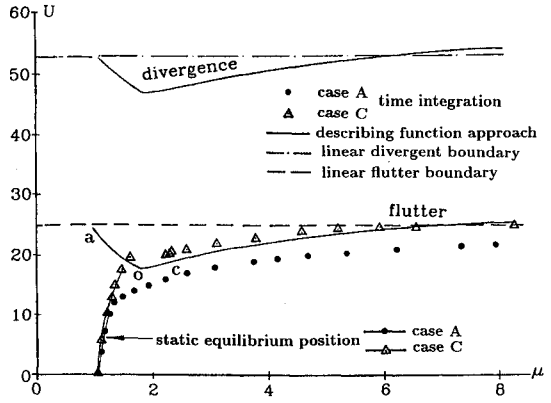

Fig. 5 Instability boundary for case A and $\theta_0 = 3$ deg.

0.1 rad. Fig. 4a is for $U = 9.5$ (m/s) and Fig. 4b is for $U = 20$ (m/s). In these cases, the motions are bounded, but when $U \geq 24.5$ (m/s), no bounded motion exists. Fig. 4a is a typical chaotic oscillation (similar to a chaotic motion of a forced buckled beam, see Holmes and Moon[9]). The condition for onset of a chaotic oscillation requires the structural parameters and airspeed to be near the lower limit cycle flutter speed region (section *aoc* shown in Fig. 3). Note that in the region where chaotic oscillations occur, the describing function approach no longer gives reliable results. Fig. 4b is a periodic limit cycle oscillation with multiple frequency components.

b. For $\theta_0 \neq 0$. The above procedure is invalid for the case, $\theta_0 \neq 0$. It is well known from Eq. (16) that δ is a function of the amplitude of oscillation as well as free stream velocity. Eqs. (16), (18), and (20) are coupled with each other. A more general approach, suitable for $\theta_0 \neq 0$, is as follows.

As a first step, we need to obtain a curve $U_F - K_{\phi eq}$ from Eq. (20). Assuming a velocity U_1, a curve (1) of $K_{\phi eq}$ vs μ can be drawn using Eqs. (16)–(18). Substituting $U_1 = U_{F1}$ into the curve of $U_F - K_{\phi eq}$, an equivalent stiffness $K_{\phi eq1}$ is determined. Corresponding to $K_{\phi eq1}$, a limit cycle amplitude ratio μ_1 is found from the curve (1). Therefore, the value U_1 with μ_1 is a solution of the nonlinear flutter equations. Repeating the above process for other U, called U_i ($i = 1, 2, 3, \ldots$), a final graph of flutter critical speed vs the ratio of limit cycle flutter amplitude is drawn as shown in Fig. 5 for $\theta_0 = 3$ deg and $\phi_a = 1$ deg. The numerical integration results for case A and case C are also shown in this figure. All the results are similar to those of Fig. 3 and are not further discussed here.

2. Forced Response ($\theta_s \neq 0$)

When a nonlinear self-excited system is subjected to an additional external excitation θ_{con} with a circular frequency Ω, then the system may respond with aperiodic or chaotic oscillations in the stable region under certain conditions. For a periodic response, a solution can be obtained using the describing function approach and an approximate iterative procedure or the Newton-Raphson algorithm. However, in addition to the periodic response, a chaotic oscillation is found for this nonlinear system. Fig. 6 shows forced response behavior near, but below, the instability boundary for $U = 8$ m/s, $\theta_0 = 0$ deg, $\theta_s = 1.5$ deg and $\Omega = 10$ Hz as obtained from the time integration. Fig. 6a shows the phase plane plot, and 6b shows the Poincare map of pitching motion for zero initial condition. The Poincare map is defined to be those points in the phase plane when $\sin \Omega t = 0$, and $\cos \Omega t > 0$. These instants in time are said to be determined by an external clock, because it does not depend on the motion.

Chaotic oscillations for both pitching and flap motions are found. An evident behavior is the global large oscillation around all three rest positions, $\phi = 0$, $\phi_{p+,-}$, with a small

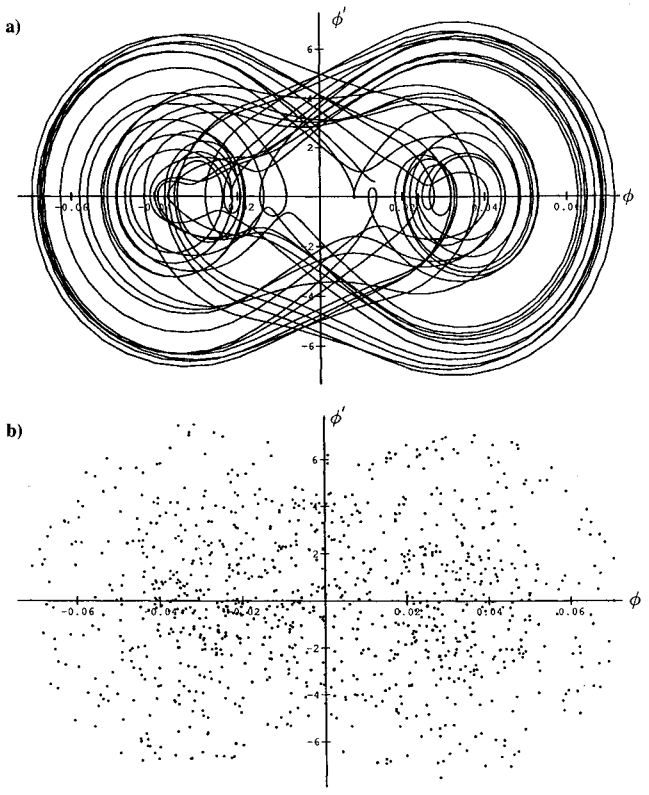

Fig. 6 Forced response for $U = 8$ m/s, $\theta_0 = 0$, $\theta_s = 1.5$ deg, and $\Omega = 10$ Hz in case A: a) for pitch phase plane plot, and b) for Poincare map of pitch motion.

fluctuation around the two equilibrium positions, $\phi_{p+,-}$. Comparing behavior of the flap and torsional response, the pitching motion is more dominant. The Poincare map includes 1000 points over 1000 driving cycles. The time interval is 0.001 s. From this figure, it is seen that the distribution of these points is diffuse.

The chaotic forced responses are only found in the lower limit cycle flutter speed region as shown in the *aoc* portion of Fig. 3. Near the high flutter speed region, the forced responses appear to be periodic.

B. Case B (Linear Blade Structure with Nonlinear Aerodynamics)

Eqs. (8) and (9) are second-order, ordinary differential equations with variables, β and ϕ, respectively. Two state variables are required for the flapping degree of freedom, and the same for the pitch motion. Equations (6) and (7) together represent a third-order system, thus three state variables are required per section for each equation. The total number of state variables is $6N + 4$. The following state vector $\{q\}$ is introduced into Eqs. (4)–(9) which serves to reduce the system to a set of $6N + 4$ first order differential equations:

$$\{q\}^T = \lfloor \beta' \beta \phi' \phi C_{lai} C_{lbi} C'_{lbi} C_{mai} C_{mbi} C'_{mbi} \rfloor \qquad (21)$$

where C_{lai}, C_{lbi} are the linear and nonlinear lift coefficient of the ith aerodynamic element, and C_{mai}, C_{mbi} are for the pitch moment coefficients. The resulting system of the state variable equations is given by

$$\{q'\} = [A]\{q\} + \{F\} \qquad (22)$$

Equation (22) is a set of nonlinear differential equations, and the solution can be obtained by numerical time integration. Note the velocity components, U_{Pi} and U_{Ti}, involve the state variables β and ϕ. The initial values of U_{Pi} and U_{Ti} are determined by initial values of the state variables that then

Table 2

a_{0l}	5.73		
a_0	1.0	b_1	−0.036618
a_1	0.1	b_2	−0.036618
a_2	0.017872506	b_3	−0.0807134
a_3	−0.01257894	b_4	−0.0052712
a_4	0.0011938905	b_5	−0.123103
a_5	$0.85338033 \times 10^{-5}$	b_6	−0.0095512

change during the numerical integration in a time-step fashion.

The blade section is a NACA 0012 airfoil. The static lift and pitch moment coefficients are identified from the experimental data using curve fitting.[10] The static aerodynamic model is described as follows:

$$C_{ls} = \begin{cases} a_{0l}\alpha & -4 \text{ deg} < \alpha < 10 \text{ deg} \\ \sum_{i=0}^{5} a_i(\alpha - 10 \text{ deg})^i & 10 \text{ deg} \le \alpha < 15.6 \text{ deg} \\ 1.13255e^{-0.01(\alpha - 15.6)} & 15.6 \text{ deg} \le \alpha \end{cases} \tag{23}$$

$$C_{ms} = \begin{cases} 0 & -6 \text{ deg} < \alpha < 13 \text{ deg} \\ (b_1 + b_2(\alpha - 13))(\alpha - 13)^2 & 13 \text{ deg} \le \alpha < 16 \text{ deg} \\ b_3 + b_4(\alpha - 16) & 16 \text{ deg} \le \alpha < 24 \text{ deg} \\ b_5 + b_6(\alpha - 24) & 24 \text{ deg} \le \alpha \end{cases} \tag{24}$$

The coefficients, $a_1, a_2, \ldots, b_1, b_2, \ldots$, are given in Table 2.

The following results are for the blade divided into four equal length strips with $\Delta_i = 0.25$.

The flutter instability boundary is significantly dependent on the initial pitch angle θ_0, as shown in Fig. 7 which gives the flutter instability boundary vs the initial pitch angle θ_0. The flutter critical speed decreases with increasing θ_0 because of the aerodynamic nonlinearity at high angle of attack. Corresponding to points near, but below the flutter boundary, the motions appear as limit cycle oscillations.

Usually the force responses are periodic motions with a fundamental period determined by the excitation frequency Ω. However, under certain conditions a chaotic oscillation may be found in a rather narrow parameter range. Fig. 8a shows the phase plane plot of the pitch motion under external harmonic excitation with $U = 20.4$ m/s, $\theta_0 = 7.8$ deg, $\theta_s = 3$ deg, and $\Omega = 11$ Hz. The motion appears to be chaotic and quite complex including several dominant frequency components. This chaotic response can be explained by Fig. 8b. Figure 8b shows the Poincare map of the aerodynamic lift coefficients vs the effective angle of attack. This Poincare map is for an external clock when $\sin \Omega t = 0$ and $\cos \Omega t > 0$. The local angle of attack at $\bar{r}_i = 0.875$ has a large variable range (−5–28 deg) as shown in this figure, and the corresponding natural frequency of the aerodynamic model varies from 12.27 to 34 Hz which exceeds the excitation frequency (11 Hz). Thus the airfoil is well into its stall regime and the aerodynamic forces have also changed the effective stiffness of the mechanical system. These severe nonlinearities are the cause of the chaotic motion.

C. Case C (Nonlinear Blade Structure with Nonlinear Aerodynamics)

Both aerodynamic and structural nonlinearities are considered in case C. Numerical integration is used to study flutter instability and forced response behavior. The aerodynamic model and nonlinear structural parameters chosen are the same as those of case B and case A. Two major issues are discussed here, the effect of initial pitch angle on flutter instability and the effect of initial conditions on forced response.

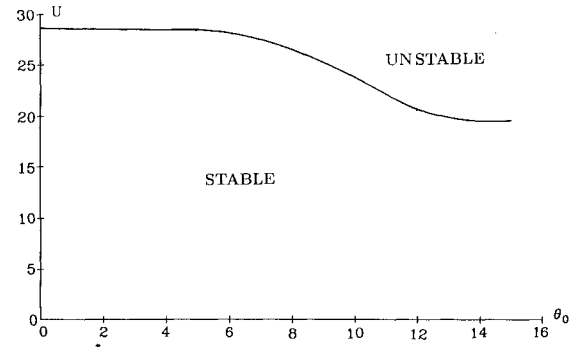

Fig. 7 Instability boundary vs θ_0 for case B.

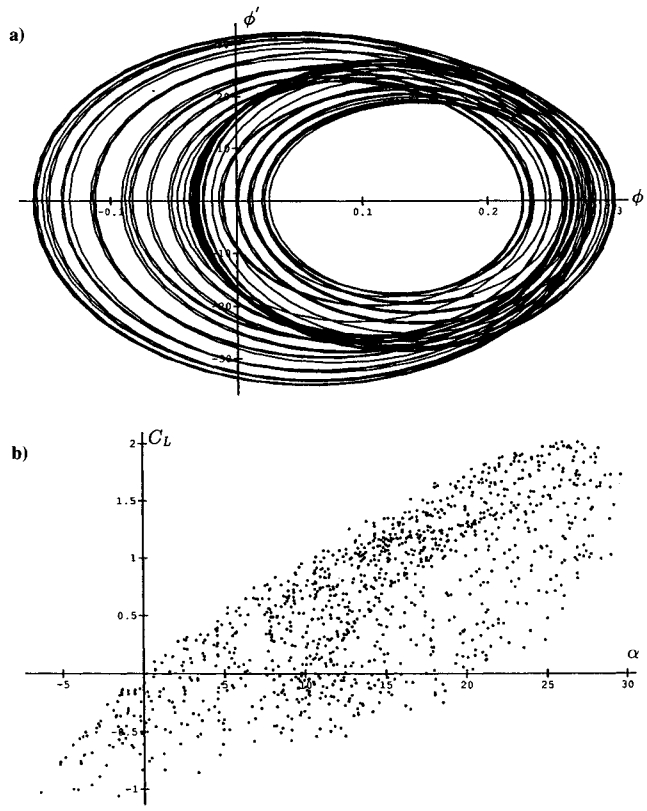

Fig. 8 Forced response of pitch motion for $U = 20.4$ m/s, $\theta_0 = 7.8$, $\theta_s = 3$ deg, and $\Omega = 11$ Hz in case B: a) for phase plane plot, and b) for Poincare map of $\alpha - C_L$.

1. *Effect of Initial Pitch Angle on Flutter Instability*

Figure 9 shows the limit cycle amplitude ratio μ vs the initial pitch angle θ_0, for $U = 10$ (curve a), 14(b), 18(c), and 22(d) m/s with initial value $\phi(0) = 0.05$ rad. The points connected by a solid line indicate the system is stable and convergent to a static equilibrium position. The unconnected symbols ●, △, ⊙, and ⊗ indicate that the system tends to a limit cycle oscillation. It is found that the equilibrium deformation increases as both θ_0 and U increases. Note that the static aerodynamic force and moment increase approximately in proportion to θ_0 and U^2, as shown in Eq. (16). A limit cycle oscillation exists when the system parameters are near the flutter instability boundary (or slightly higher than the flutter critical speed). This is because the aerodynamic model has a larger hysteretic aerodynamic damping in both flap and pitch motions as stall occurs or the structure has freeplay nonlinear torsional stiffness. Extreme large freestream velocity and initial pitch angle, such as $U > 22$ m/s and $\theta_0 > 11$ deg, will lead the system to be divergent. Also note from Fig. 9 that the limit cycle amplitude increases with increasing U and θ_0.

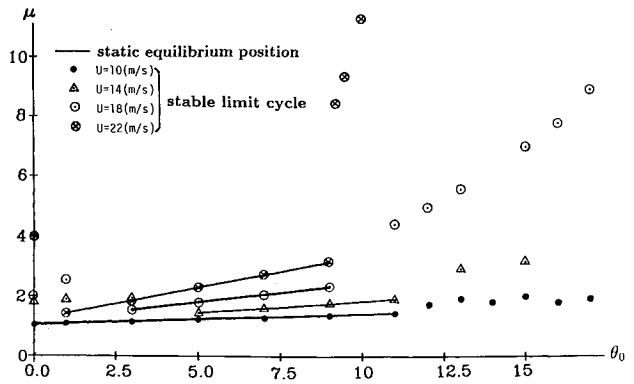

Fig. 9 Limit cycle ampliture ratio vs θ_0 for U = 10, 14, 18, and 22 m/s in case C.

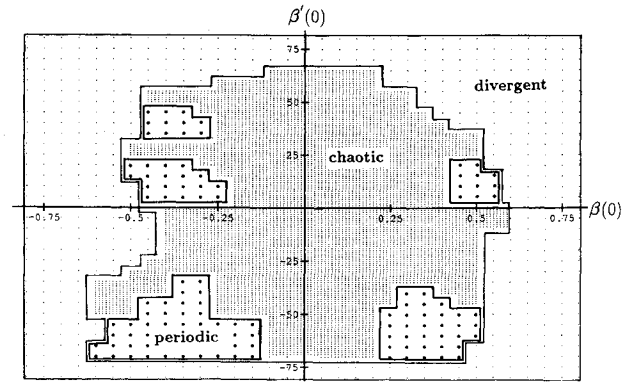

Fig. 10 Pitch initial condition map for U = 12 m/s, θ_0 = 1 deg, θ_s = 1.5 deg, and Ω = 11 Hz in case C.

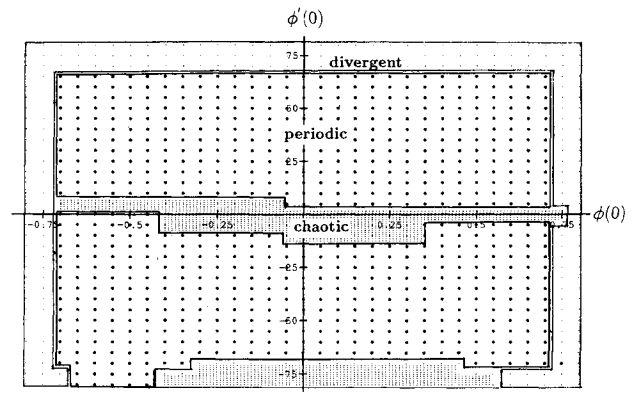

Fig. 11 Flap initial condition map for U = 12 m/s, θ_0 = 1 deg, θ_s = 1.5 deg, and Ω = 11 Hz in case C.

For $\theta_0 = 0$, the flutter instability boundary is plotted in Fig. 3 for comparison with that from case A. There is an evident difference between the two cases, A and C. The critical speeds obtained from case C are higher than those from case A. Although the angle of attack is within the linear region of the static aerodynamic coefficients, the aerodynamic model in case C still provides hysteretic behavior (aerodynamic damping) due to the interaction of structural nonlinearity and the aerodynamic forces.

2. Effect of Initial Conditions on Forced Response

The motion is quite sensitive to the initial conditions. Two typical examples are studied. One is for the case with lower U and θ_0, and another is for higher U and θ_0. As a first example, Figs. 10 and 11 show how the flap and pitch motion behavior varies with various initial disturbance amplitudes for θ_0 = 1 deg, θ_s = 1.5 deg, Ω = 11 Hz, and U = 12 m/s,

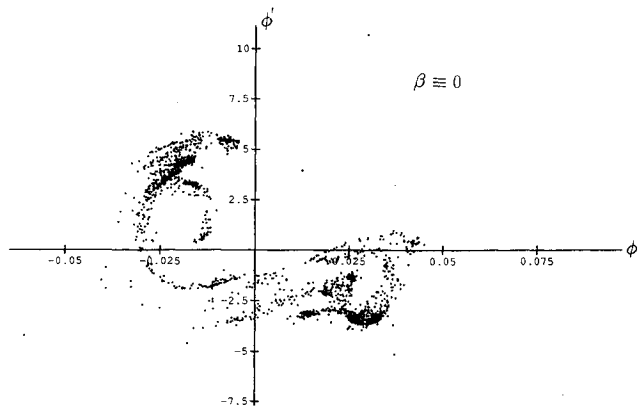

Fig. 12 Poincare section map for an internal clock at those times when $\beta \equiv 0$, in case of U = 12 m/s, θ_0 = 1 deg, θ_s = 1.5 deg, and Ω = 11 Hz, $\phi(0)$ = 0.1 rad, $\phi'(0)$ = −5 rad/s in case C.

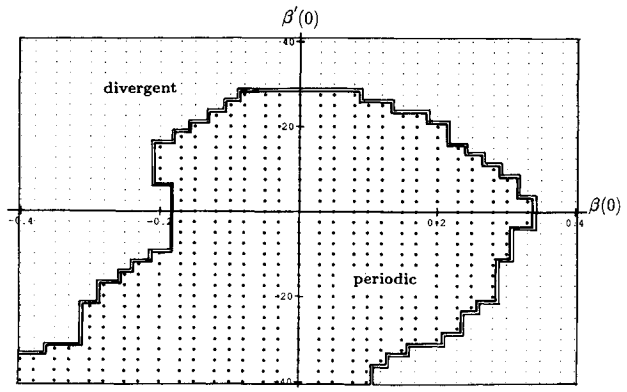

Fig. 13 Pitch initial condition map for U = 16 m/s, θ_0 = 9 deg, θ_s = 3 deg, and Ω = 11 Hz in case C.

respectively. In varying the initial conditions, all initial variables were set to zero except for $\phi(0)$ and $\phi'(0)$, or $\beta(0)$ and $\beta'(0)$. Each point in these figures represents the motion behavior which is identified by a Poincare map of over 1100 points in which the long time steady state results are obtained. The abscissae displays the initial pitch angle (or flap angle) from −0.8 to 0.8 rad. The ordinate displays the initial pitch rate (or flap rate) from −80 to 80 rad/s. There are three kinds of motion shown in these figures, periodic, chaotic, and divergent. The periodic motion is indicated by the symbol of (•). The divergent motion is indicated by the symbol of small dots (·) and the chaotic motion by the shaded region. From Figs. 10 and 11, the distinct difference among the locations of the periodic, chaotic, and divergent regions shows the system's sensitivity to the initial disturbance. For this case, the chaotic motion is more sensitive to the flap initial conditions than to the pitch initial conditions, compare Fig. 10 and Fig. 11. These results are broadly similar to those of Ventres and Dowell[11] for a different aeroelastic system. For a certain set of system parameters, initial conditions can play an important role.

Figure 12 shows a typical Poincare section map of the pitching motion for an internal clock, i.e., at those times when $\beta \equiv 0$. This figure is for the pitch initial condition, $\phi(0)$ = 0.1 rad, $\phi'(0)$ = −5 rad/s. There are 2200 points distributed in two regions for 100 s long time series and a time step of 0.001 s in this figure. Note that there are two times per excitation period when $\beta = 0$. The pitching responses still appear to be chaotic as shown in Figs. 10 and 11. Also it is seen from these figures that a different initial condition leads to a different chaotic Poincare map for the same internal clock.

As a second example, Figs. 13 and 14 show that the flap and pitch motion behavior varies with the various initial dis-

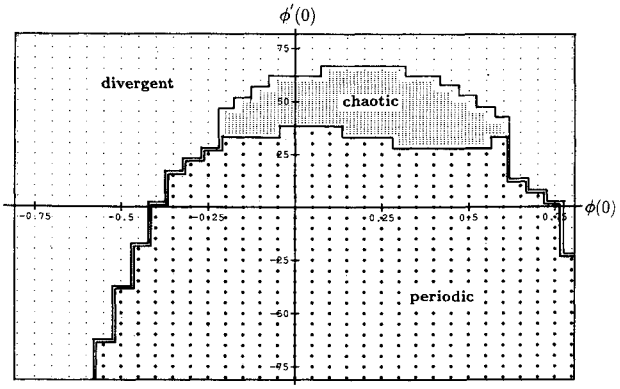

Fig. 14 Flap initial condition map for U = 16 m/s, θ_0 = 9 deg, θ_s = 3 deg, and Ω = 11 Hz in case C.

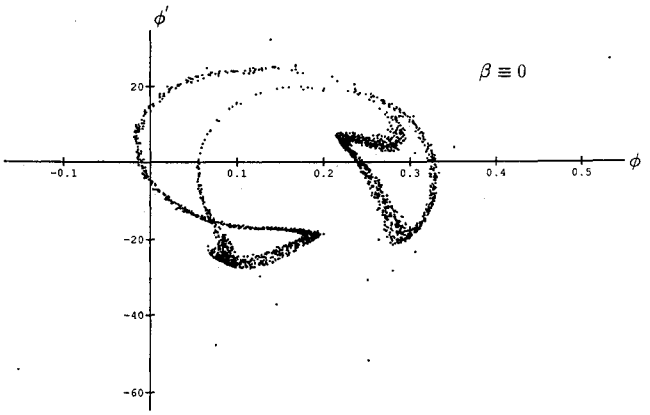

Fig. 15 Poincare section map for an internal clock at those times when $\beta \equiv 0$, in case of U = 16 m/s, θ_0 = 9 deg, θ_s = 3 deg, and Ω = 11 Hz, $\phi(0)$ = 0.5 rad, $\phi'(0)$ = 40 rad/s in case C.

turbance amplitudes for θ_0 = 9 deg, θ_s = 3 deg, Ω = 11 Hz, and U = 16 m/s, respectively. Figure 13 shows the initial condition map for the $\phi(0) - \phi'(0)$ plane, and Fig. 14 for the $\beta(0) - \beta'(0)$ plane. A common characteristic of the initial Poincare maps for Figs. 10, 11, and 13 is that a certain initial disturbance is able to lead to a chaotic oscillation; but that is not the case in Fig. 14.

The motion behavior of Fig. 13 is very similar to that of case B as shown in Fig. 8. This means that the chaotic oscillation is dominated by nonlinear aerodynamic stall. From Fig. 13 it is seen that most chaotic motions occur in the first quadrant of the pitch initial conditions. No chaotic motion exists in the third and fourth quadrants. Also, as noted above, no chaotic motion occurs in any of the quadrants for the flap initial conditions: $\beta(0)$, from -0.4 to 0.4 rad, and $\beta'(0)$, from -40 to 40 rad/s. The distinct difference between Fig. 13 and Fig. 14 again shows the significant effects of the initial disturbance on the response characteristics.

Figure 15 shows the Poincare section map of the pitching motion for an internal clock when $\beta \equiv 0$ and the pitch initial conditions, $\phi(0)$ = 0.5 rad and $\phi'(0)$ = 40 rad/s. There are 2372 points distributed in $\phi - \phi'$ plane in which there are more than two times per excitation period when β = 0. The pitching response appears to be chaotic.

If the freestream velocity U increases but remains below the flutter critical speed (such as U = 18 m/s), it is found that the response motion is dominated by chaos; however, the initial disturbance amplitude still has an effect on response behavior.

IV. Concluding Remarks

Structural and aerodynamic nonlinearities will often lead to a limit cycle flutter oscillation. The limit cycle flutter amplitude is primarily dependent upon the freestream velocity, initial pitch angle, the magnitude of the deadspace of the freeplay structural nonlinearity, and the initial conditions. The motion behavior (periodic, aperiodic, or chaotic motion) is quite sensitive to the initial disturbance for forced response. Therefore, for both structural and aerodynamic nonlinear systems, the initial conditions should be considered as a significant factor.

Chaotic motion may be found from both unforced and forced response analysis when the motion is near the flutter boundary or when stall occurs. Near the region of low-limit cycle flutter speed, the chaotic behavior is dominated by the effect of structural nonlinearity. However, near the region of high-limit cycle flutter speed, the chaotic oscillation is dominated by aerodynamic stall nonlinearity. When the condition for the onset of chaotic motion is satisfied, both flapping and pitching motions appear to have chaotic oscillations; however, the pitching vibrations are more dominant than those for flapping.

Appendix: Coefficients of Eq. (20)

$$
\begin{aligned}
a_{11} &= 1 + s_l\gamma\bar{c}/12a_{0l} \\
a_{12} &= -\bar{I}_y - \gamma\bar{c}^2\pi/32a_{0l} \\
a_{21} &= -\bar{I}_y - \gamma\bar{c}^2(\pi/32 + s_l\bar{y}_{ac}/4)/a_{0l} \\
a_{22} &= \bar{I}_f + \gamma\bar{c}^3(3\pi/128 + \bar{y}_{ac}\pi/16)/a_{0l} \\
b_{11} &= \gamma/6R \\
b_{12} &= -s_l\gamma\bar{c}/8a_{0l}R \\
b_{21} &= -\bar{y}_{ac}\gamma\bar{c}/4R \\
b_{22} &= \gamma\bar{c}^2(\pi/16 + s_l\bar{y}_{ac}/4)/a_{0l}R \\
c_{11} &= \omega_\beta^2 \\
c_{12} &= -\gamma/4R^2 \\
c_{20} &= \bar{I}_f\omega_\phi^2 \\
c_{22} &= \gamma\bar{c}y_{ac}/2R^2 \\
d_0 &= a_{11}b_{22} + b_{11}a_{22} - a_{12}b_{21} - a_{21}b_{12} \\
d_1 &= (b_{11}c_{22} - b_{12}c_{12})/d_0 \\
d_2 &= b_{22}c_{11}/d_0 \\
d_3 &= b_{11}/d_0 \\
d_4 &= a_{11}a_{22} - a_{12}a_{21} \\
d_5 &= a_{11}c_{22} + b_{11}b_{22} - a_{21}c_{12} - b_{21}b_{12} \\
f_1 &= d_1^2d_4 - d_1d_5 \\
f_2 &= 2d_1d_3d_4 - a_{11}d_1 - d_3d_5 \\
f_3 &= 2d_1d_3d_4 + c_{11}c_{22} - a_{22}c_{11}d_1 - d_2d_5 \\
f_4 &= d_3^2d_4 - a_{11}d_3 \\
f_5 &= 2d_2d_3d_4 + c_{11} - a_{22}c_{11}d_3 - a_{11}d_2 \\
f_6 &= d_2^2d_4 - a_{22}c_{11}d_2 \\
s_l &= 0.09(180/\pi)
\end{aligned}
$$

Acknowledgments

This work was supported by the Army Research Office under Grant DAAL03-87-K-0023; Gray Anderson is the technical monitor. All numerical simulations were done on a supercomputer, the Cray Y-MP of the North Carolina Supercomputing Center (NCSC).

References

[1]Dunn, P., and Dugundji, J. "Nonlinear Stall Flutter and Divergence Analysis of Cantilevered Graphite/Epoxy Wings," AIAA Paper 90-0983-CP, 1990.

[2]Tang, D. M., and Dowell, E. H., "Comparison of Theory and Experiment for Nonlinear Flutter and Stall Response of Helicopter Blade," *Proceedings of 47th Annual Forum of American Helicopter Society,* May, 1991, pp. 1413–1425.

[3]Tran, C. T., and Falchero, D., "Application of the ONERA Dynamic Stall Model to a Helicopter Blade in Forward Flight," *Vertica,* Vol. 6, 1982, pp. 219–239.

[4]Brase, L. O., and Eversman, W., "Application of Transient Aerodynamics to the Structural Nonlinear Flutter Problem," *Journal of Aircraft,* Vol. 25, No. 11, 1988, pp. 1060–1068.

[5]Yang, Z. C., and Zhao, L. C., "Analysis of Limit Cycle Flutter of an Airfoil in Incompressible Flow," *Journal of Sound and Vibration,* Vol. 23, No. 1, 1988, pp. 1–13.

[6]Anthony, J. H., et al., "Chaotic Response of Aerosurfaces with Structural Nonlinearities," AIAA Paper 90-1034-CP, 1990.

[7]Petot, D., and Dat, R., "Unsteady Aerodynamic Loads on an Oscillating Airfoil with Unsteady Stall," 2nd Workshop on Dynamics and Aeroelasticity Stability Modeling of Rotorcraft Systems, Florida Atlantic, Boca Raton, FL, Nov. 1987.

[8]Laurenson, R. M., and Trn, R. M., "Flutter Analysis of Missile Control Surfaces Containing Structural Nonlinearities," *AIAA Journal*, Vol. 18, No. 10, 1980, pp. 1245–1251.

[9]Holmes, P. J., and Moon, F. C., "Strange Attractors and Chaos in Nonlinear Mechanics," *Journal of Applied Mechanics*, Vol. 50, 1983, pp. 1021–1032.

[10]Carta, F. O., and Niebanck, C. F., "Prediction of Rotor Instability at High Forward Speed. Vol. III, Stall Flutter," U. S. Army Aviation Labs TR 68-18C.

[11]Ventres, C. S., and Dowell, E. H., "Comparison of Theory and Experiment for Nonlinear Flutter of Loaded Plates," *AIAA Journal*, Vol. 8, 1970, pp. 2022–2030.